

# PCCP

Accepted Manuscript



This is an *Accepted Manuscript*, which has been through the Royal Society of Chemistry peer review process and has been accepted for publication.

*Accepted Manuscripts* are published online shortly after acceptance, before technical editing, formatting and proof reading. Using this free service, authors can make their results available to the community, in citable form, before we publish the edited article. We will replace this *Accepted Manuscript* with the edited and formatted *Advance Article* as soon as it is available.

You can find more information about *Accepted Manuscripts* in the [Information for Authors](#).

Please note that technical editing may introduce minor changes to the text and/or graphics, which may alter content. The journal's standard [Terms & Conditions](#) and the [Ethical guidelines](#) still apply. In no event shall the Royal Society of Chemistry be held responsible for any errors or omissions in this *Accepted Manuscript* or any consequences arising from the use of any information it contains.

Cite this: DOI: 10.1039/c0xx00000x

www.rsc.org/xxxxxx

ARTICLE TYPE

# Influence of process variables on extraction of Cefalexin in a novel biocompatible ionic liquid based-aqueous two phase system †

Shiva Abdolrahimi<sup>a</sup>, Bahram Nasernejad<sup>\*a</sup> and Gholamreza Pazuki<sup>a</sup>*Received (in XXX, XXX) Xth XXXXXXXXX 20XX, Accepted Xth XXXXXXXXX 20XX*

DOI: 10.1039/b000000x

Despite the fact that ionic liquid-based aqueous two phase systems (ATPS) have been widely studied for extraction purposes, the adequacy of biodegradable organic salts as salting out agents has been left unexploited. In this study, we investigated the ability of sodium-based organic salts in the formation of ATPS in the presence of a common ionic liquid, [C<sub>4</sub>mim]BF<sub>4</sub>. In the pioneer aspect of this work, Response Surface Methodology (RSM) based on three-variable central composite design (CCD) was employed for determination of the effect of pH and the initial concentration of phase components on partition coefficient of Cefalexin. Consequently, regression model equations and contour plots were applied to evaluate the effect of system's parameters on biomolecule's extraction. The tie-line (TL) data were determined for each experimental run and their reliability was confirmed by Othmer-Tobias and Bancroft correlations. In order to investigate the salting-out ability the effective excluded volume (EEV) was determined from the binodal data. Furthermore, FTIR spectra confirmed no chemical interactions between Cefalexin and [C<sub>4</sub>mim]BF<sub>4</sub> in the extraction process. The microscopic structure of the top phase was analyzed by DLS, conductivity and TEM in order to investigate the mechanism of extraction. Hydrophobic interaction, salting-out effect and the aggregation phenomena played the dominant role in the study of extraction process.

## 1. Introduction

The growing demand for pure biotechnologically manufactured chemicals has made their separation and purification of great industrial importance. Furthermore, production costs are entirely related to the underlying separation process. Liquid-liquid extraction techniques propose some unique features suitable for bioseparation. Among those high yields, improved selectivity, high effectiveness, and high purity degree are worth noting [1]. Regarding the fact that most biomolecules of interest are manufactured in aqueous media, organic solvents have been widely used for purification purposes. Consequently, their high volatility and toxicity impose some hazardous effects on the environment. As a result, the improvements of new and "greener" separation techniques have been an interesting research platform in the past decades [1]. In the mid-1950's, Albertsson introduced "Aqueous Two Phase System" (ATPS) as a novel method replacing the conventional liquid-liquid extraction technique [2]. The ATPS is mostly composed of two immiscible aqueous-rich phases which are mainly formed by the addition of structurally different polymers, a polymer and a salt, or two salts [1,3]. Since the bulk of both phases is mainly composed of water, ATPS provides a gentle and compatible media for biomolecules [2-4]. Moreover, as the two immiscible phases possess some

unique physical and chemical properties, the biomolecules are favourably partitioned between phases. Accordingly, since the pioneer work of Albertsson [5], polymer-based ATPS have been broadly applied to the recovery and purification of biomolecules [6-11].

The innovative research work of Rogers and co-workers in 2003 proposed a novel system of Ionic Liquid (IL) –inorganic salt for the formation of ATPS [12]. The distinct physical and chemical properties of ILs such as non-flammability, tunability, negligible vapor pressure, high selectivity, and a large liquid range make them a reliable choice for industrial application [1,2]. Consequently, their negligible volatility and non-flammability characterize them under the common "green solvents" group. Recently, a large set of literature has been aimed for applications of ILs as a viable alternative to polymer based ATPS [13-18]. The major favourable aspect of IL-based over polymer-based ATPS is the possibility to tailor their polarities by a suitable manipulation of cation-anion combinations [3]. Nonetheless, a large number of studies have applied inorganic salts based on phosphate, sulphates, and carbonate anions [19-22] as the salting-out agents in ATPS formation. However, high concentration discharges of these salts in the effluent streams propose some hazardous environmental concerns. As a result, recent research studies have focused on the application of

biodegradable such as tartrate-, citrate-, or acetate-based organic salts as salting out agents [17, 23-28].

Conventional methods of studying a process, beside being time consuming and requiring a large number of experiments, involve maintaining other factors at an unspecified constant level; therefore, the interaction among the variables is not studied [29,30]. Thus, in order to eliminate the limitations of conventional methods a statistical experimental design such as RSM is developed. RSM is a useful tool for developing, improving and optimizing processes while evaluating the significance of several affecting parameters. Also, it enables us to study the interaction among the variables even in the presence of complex interactions.

Considering the fact that organic salts are biodegradable and they are scarcely studied, we investigated salting-out ability of some sodium-based organic salts as a novel alternative in the presence of a common ionic liquid. In addition, Cefalexin was the selected biomolecule to prove the applicability of these systems for extraction purposes. Feed initial ionic liquid and organic salt's concentrations along with its pH are important parameters effecting biomolecule's partitioning in IL-based ATPS. Many research studies have combined the conductivity, DLS and TEM to investigate the microstructure of ATPS and the possible mechanism for the extraction [31-36]. Recently, TEM was used to characterize the appearance of aggregates in aqueous solution of various ILs [35, 36]. Also, the possible mechanisms for biomolecule's extraction have been related to microstructure of the IL-rich phase. Thus, in the present study, capacity of IL-organic salt ATPS in partitioning of Cefalexin was investigated by varying these factors using face centred CCD method. Interactions among these factors were investigated and regression equations were evaluated. In addition, FTIR, DLS, conductivity and TEM were employed to study the mechanism of extraction process.

## 2. Materials and methods

### 2.1. Materials

The detailed properties of all the materials used in this work are presented in Table 1. The chemicals were used without further purification and doubled distilled deionized water was used to prepare the samples.

### 2.2. Experimental Procedure

#### 2.2.1. Phase Diagrams

Visual determination of cloud points has been employed in most research studies for determination of the binodal curve [7-27]. Hence, the phase diagrams were determined by employing cloud point titration method at  $25 \pm 1$  °C and atmospheric pressure. Aqueous solution of tri-sodium citrate 5,5-hydrate at 40 wt%, disodium tartrate dihydrate, disodium succinate hexahydrate, and disodium fumarate at 25 wt%; and  $[C_4mim]BF_4$  at 80 wt% were prepared and used for determination of the binodal curves.

The experimental procedure consists of two steps: (i) drop-wise addition of each aqueous organic salt solution to ionic liquid's aqueous solution until the detection of a cloudy (biphasic) solution; (ii) drop-wise addition of ultra-pure water until the formation of a monophasic region (limpid solution). The systems'

compositions at each point were determined by weight quantification within  $\pm 10^{-4}$  g. In order to complete the phase diagrams, ionic liquid's aqueous solution were also added to the salt solutions.

The experimental binodal curves were fitted to the following four-parameter equation [3]:

$$[IL] = \exp(A + B[salt]^{0.5} + C[salt] + D[salt]^2) \quad (1)$$

Where [IL] and [salt] are mass fraction percentage of the ionic liquid and organic salts, respectively, and A, B, C, and D are fitting parameters obtained by data regression.

#### 2.2.2. Determination of TLs

Merchuk et al. [37] initially introduced a gravimetric method for determination of TLs of polymer-based ATPS. Later, Rogers and co-workers [12] successfully employed this method for IL-based ATPS. In this method, binodal data by equation 1 are coupled with mass balance relationships thus, compositions of the top and bottom phases are determined by lever-arm rule. Therefore, for each TL, the following system of four equations and four unknown values (which correspond to  $[IL]_{top}$ ,  $[IL]_{bot.}$ ,  $[salt]_{top}$ ,  $[salt]_{bot.}$ ) was solved:

$$[IL]_{top} = \exp(A + B[salt]_{top}^{0.5} + C[salt]_{top} + D[salt]_{top}^2) \quad (2)$$

$$[IL]_{bot} = \exp(A + B[salt]_{bot}^{0.5} + C[salt]_{bot} + D[salt]_{bot}^2) \quad (3)$$

$$[IL]_{top} = \frac{[IL]_M}{\alpha} - \frac{1-\alpha}{\alpha} [IL]_{bot} \quad (4)$$

$$[salt]_{top} = \frac{[salt]_M}{\alpha} - \frac{1-\alpha}{\alpha} [salt]_{bot} \quad (5)$$

Where subscripts "top", "bot.", and "M" refer to the top-phase, the bottom-phase and the mixture, respectively; [IL] and [salt] designate mass fraction percentage of ionic liquid and salt in the solution. Furthermore,  $\alpha$  is known to be the ratio between the mass of the top phase and the total mass of the mixture.

The tie-line lengths (TLL) and slope of TLs (STL) were calculated by the following equations:

$$TLL = \sqrt{([IL]_{top} - [IL]_{bot})^2 + ([salt]_{top} - [salt]_{bot})^2} \quad (6)$$

$$STL = \frac{[IL]_{top} - [IL]_{bot}}{[salt]_{top} - [salt]_{bot}} \quad (7)$$

#### 2.2.3. DOE

The Classical and conventional methods of studying a process are carried out by varying a single factor while maintaining all the other factors at an unspecified constant level. These methods, beside being time consuming and requiring large number of experiments, do not give combined effect of process variables [29]. Moreover, they require a large number of experiments to evaluate optimum levels while they are incapable of effective optimization. Considering the limitations of conventional

methods, a statistical experimental design such as RSM, which optimizes all the affecting parameters, can be promising [29,38]. RSM is a collection of statistical and mathematical techniques which evaluates the regression models and determines the effect of variables even in the presence of complex interactions [39,40]. The main objective of RSM is evaluation of the optimum operational conditions for the system or determination of a region that satisfies the desired specifications [29,39]. CCD is a well known standard RSM design; which we applied in this work to study the variables that affect the partitioning of the Cefalexin. Generally, the CCD consists of  $2n$  axial runs with  $2^n$  full factorial runs and also  $n_c$  replicates at the center points. The center point replicates are a reliable indication of precision property and experimental error; moreover, they prove reproducibility of the data.

A central composite face centered design was employed in order to investigate the effect of different parameters of the system on the partitioning of Cefalexin in IL-organic salt ATPS. The independent variables selected in this study were (i)  $X_1$ : initial pH of the feed; (ii)  $X_2$ : organic salt's mass fraction percentage in the feed; (iii)  $X_3$ : IL's mass fraction percentage in the feed and partitioning coefficient of Cefalexin (equation 8) was dependent output response variable.

$$K_{Cef} = \frac{[Cef.]_{IL}}{[Cef.]_{salt}} \quad (8)$$

Where  $[Cef.]_{IL}$  is the concentration of Cefalexin in the IL-rich phase and  $[Cef.]_{salt}$  is its respective concentration in the organic salt-rich phase. Moreover, the extraction efficiency for Cefalexin enrichment is determined in accordance with equation 9:

$$\%EE_{Cef} = \frac{100}{1 + \frac{1}{R_v K_{Cef}}} \quad (9)$$

Where  $R_v$  is the phase volume ratio which is determined by dividing the volume of top phase to that of the bottom phase.

Thus  $2^3$  full factorial CCD for 3 variables,  $2 \times 3$  axial points and 2 replicates at the center points were employed resulting 16 as the total number of experiments.

The independent variables,  $X_i$ , are coded as  $x_i$ , according to the following relationship:

$$x_i = \frac{(X_i - X_0)}{\partial X} \quad (10)$$

Where  $x_i$  is the coded value of  $i$  th independent variable,  $X_i$  the natural value of  $i$  th independent variable,  $X_0$  the natural value of the  $i$  th independent variable at the center point, and  $\partial X$  is the value of step.

Table 2 shows independent variables and their coded and uncoded levels for all investigated organic salt-IL ATPSs. Moreover, this table manifests the fact that for each organic salt the feed's mass fraction percentage varies as the binodal changes. An empirical model, which is a mathematical relationship between the response and the independent variables, is of great importance in the study of a process. Each set of responses is used to develop an empirical model using a second degree

polynomial equation; as given by the following equation:

$$Y = b_0 + \sum_{i=1}^n b_i x_i + \sum_{i=1}^n b_{ii} x_i^2 + \sum_{i=1}^{n-1} \sum_{j=i+1}^n b_{ij} x_i x_j \quad (11)$$

Where  $Y$  is the predicted response,  $b_0$  the constant coefficient,  $b_i$  the linear coefficients,  $b_{ii}$  the quadratic coefficients,  $b_{ij}$  the interaction coefficients and  $x_i$ ,  $x_j$  are the coded values of independent process variables.

Table 4 demonstrates the complete design matrix of the performed experiments. The IL-based ATPS was prepared by mixing appropriate amount of  $[C_4mim]BF_4$  and organic salts to get the required composition in DOE table. Moreover, a suitable amount of Cefalexin was added to get the concentration of 0.01 g/mL. All mixtures were gravimetrically prepared within  $\pm 10^{-4}$  g. Sulfuric acid and Sodium hydroxide were used to adjust the pH of aqueous solutions to the desired values. Consequently, the prepared mixtures were vigorously stirred and kept in small decanters for 48hr for complete phase separation. In order to eliminate the effect of temperature, all samples were incubated at  $25 \pm 1$  °C. Additionally, the same mass fraction percentages were used for TL determinations.

The regression and graphical analysis was performed by MINITAB 16 statistical software.

## 2.3. Analytical techniques

### 2.3.1. UV Spectroscopy

UV spectroscopy was employed in order to determine the concentration of Cefalexin in each phase after establishment of equilibrium. In order to obtain the wavelength corresponding to the maximum absorbance ( $\lambda_{max}$ ), a standard solution of the Cefalexin was taken and the absorbance was determined at different wavelengths by UV-Vis spectrophotometer (Jasco V-550). The plotted graph of absorbance versus wavelengths indicated  $\lambda_{max}$  to be equal to 261nm. Slight interferences of the organic salts and the ionic liquid in the quantification of Cefalexin were verified. Furthermore, in order to avoid such interferences, all samples were analyzed against blanks which have the same composition but lack antibiotic.

### 2.3.2. FTIR analysis

The surface functional group of the samples was confirmed by Fourier Transform Infrared (FTIR) spectroscopy (Nexus 670-FTIR ESP). Accordingly, FT-IR spectra of pure Cefalexin, pure IL, and Cefalexin in IL-rich top phase were recorded in absorption range of 4000 to 400  $cm^{-1}$ .

### 2.3.3. Conductivity, DLS and TEM

Electrical conductivity was measured by WTW Cond 3110 (Germany) at  $25 \pm 1$  °C. Conductivity of different concentrations of IL solution was recorded when its stability was better than 1% within 2 min intervals.

Dynamic Light Scattering (DLS) method is a technique for measuring particle size typically in the sub micron region. Thus, DLS of pure aqueous solution of Cefalexin, IL rich top phase without Cefalexin and Cefalexin in IL rich top phase have been recorded. We analyzed the samples by ZEN 3600 DLS (Malvern, UK). The measurements were performed at  $25 \pm 1$  °C.

Moreover, the microscopic structures of the samples were

analyzed by Zeiss (Germany, 100 KV). Consequently, a small drop of each sample solutions was dripped on a copper grid. After application of a filter paper to remove the excess liquid, the samples were dried and imaged under vacuum conditions.

### 3. Results and Discussion

#### 3.1. Phase Diagrams

As all the novel ATPSs share the same ionic liquid and the pressure and temperature are also common, the comparison of the data leads to the evaluation of the effect of the organic salts on ATPS creation. All the studied organic salts were able to create ATPS with [C<sub>4</sub>mim]BF<sub>4</sub>. The experimental phase diagrams for the ternary phase systems composed of [C<sub>4</sub>mim]BF<sub>4</sub> + organic salt + water are depicted in Fig. 1. The complete experimental weight fraction data of the ternary systems is lengthy and it is presented in the supporting information. In order to compare the salting-out behaviour of organic and inorganic salts some experimental studies were conducted and the results are plotted in Fig. 2. In order to avoid the influence of the divergences that could be a mere result of different molecular weight of salts, Fig. 2 is presented in molality units (Fig. 2). In all phase diagrams, the biphasic region is above the saturation curve. As a result, as the curve gets closer to the axes the biphasic area is expanded and consequently liquid-liquid demixing is facilitated *i.e.*, ionic liquid is more easily salted out by sodium-based organic salts. As can be observed, the salting-out ability of organic and inorganic salts are comparable and in some cases organic salts are more effective for liquid-liquid demixing. We found the salting out ability of organic salts in the order: C<sub>6</sub>H<sub>5</sub>O<sub>7</sub><sup>-3</sup> > C<sub>4</sub>H<sub>4</sub>O<sub>4</sub><sup>-2</sup> > C<sub>4</sub>H<sub>4</sub>O<sub>6</sub><sup>-2</sup> > C<sub>4</sub>H<sub>2</sub>O<sub>4</sub><sup>-2</sup>. This observation is justified by the fact that ion charge plays a significant role as the trivalent anion has stronger salting out ability than the divalent ones.

The salting-out inducing ions are also called “Kosmotropes” due to their ability to create water bulk structure [41-43]. However, recent studies question the fact that the change in the bulk water structure is the main influencing effect. Evidence through recent works suggests the presence of interactions between IL and salt ions. Salting-out inducing ions act primarily through an entropic effect due to the creation of hydration complexes which subsequently cause the dehydration of the solute and the increase the cavity’s surface tension [44-46].

Nonlinear regression of the experimental phase diagrams derived the parameters of equation 1, as well as the corresponding correlation coefficients and standard deviations. As it can be observed by the R<sup>2</sup>-value, it is reasonable to confirm the adequacy of equation 1 in describing the experimental data.

#### 3.2. Effective excluded volume and salting-out ability

In 1993, Guan et al. [47] proposed a binodal model based on the statistical geometry methods for aqueous solution of polymers. Their theory is based on the concept that any molecular species in a solution is distributed randomly and thus, every system composition along the binodal curve is geometrically saturated solution of each solute in the presence of other [48]. In this work, the binodal curves of [C<sub>4</sub>mim]BF<sub>4</sub>-organic salts were correlated based on EEV theory for evaluation of the salting-out ability of

the organic salts. For the ternary system of IL (1) + organic salt (2) + water (3), the excluded volume theory can be stated by two equations [48]:

$$\ln(V_{213}^* \frac{w_2}{M_2} + f_{213}) + V_{213}^* \frac{w_1}{M_1} = 0 \quad (12)$$

$$\ln(V_{213}^* \frac{w_2}{M_2}) + V_{213}^* \frac{w_1}{M_1} = 0 \quad (13)$$

Where  $V_{213}^*$ ,  $f_{213}$ ,  $M_1$ , and  $M_2$  are the scaled EEV of organic salt, the volume fraction of unfilled effective available volume after tight packing of salt molecules into the network of [C<sub>4</sub>mim]BF<sub>4</sub>, and molecular weight of IL and organic salt, respectively.

The EEV value indicates the compatibility of the components in the system as it represents the smallest space at which each IL molecule will accept an individual salt. The correlation of the experimental binodal data gives the value of EEV and  $f_{213}$  (Table 5). We observed a negligible value for  $f_{213}$  which is due to the size differences between the components. In many experimental studies [49, 50] the salting-out strength of the salts have been related to EEV. Thus, it is reasonable to conclude that the organic salts with larger values of EEV are stronger salting-out agents. Consequently, the rank order of C<sub>6</sub>H<sub>5</sub>O<sub>7</sub><sup>-3</sup> > C<sub>4</sub>H<sub>4</sub>O<sub>4</sub><sup>-2</sup> > C<sub>4</sub>H<sub>4</sub>O<sub>6</sub><sup>-2</sup> > C<sub>4</sub>H<sub>2</sub>O<sub>4</sub><sup>-2</sup> manifests the ability of anion to create a biphasic region.

#### 3.3. TL data and Correlations

The TL data were obtained for each experimental run in DOE table. Consequently, upper phase and lower phase compositions along with TLL and STL were determined with variation of independent variables at fixed temperature. For most systems, the concentration of [C<sub>4</sub>mim]BF<sub>4</sub> in the lower phase was fairly small. However, the same behaviour was not observed in the top phase.

The TLs compositions were evaluated by employing gravimetric method along with solution of a system of four equations and four unknowns. We present the resulting TLs compositions in Tables 6, 7, and 8. Moreover, Othmer-Tobias [51] and Bancroft [52] correlations have been applied for assessment of TLs for [C<sub>4</sub>mim]BF<sub>4</sub>-organic salt ATPS:

$$\ln \frac{100 - [IL]_{top}}{[IL]_{bot}} = a + b \ln \frac{100 - [salt]_{bot}}{[salt]_{top}} \quad (14)$$

$$\ln \frac{100 - [salt]_{bot} - [IL]_{bot}}{[salt]_{top}} = c + d \ln \frac{100 - [salt]_{top} - [IL]_{top}}{[salt]_{top}} \quad (15)$$

Where a, b, c and d are adjustable parameters which can be calculated from the intercept and slope of the plotted linear relationships. The values of the adjustable parameters as a function of pH with corresponding correlation coefficients and standard deviations are presented in Table 9. On the basis of reported R<sup>2</sup>-values in Table 9, it can be concluded that these correlations can be satisfactorily used to correlate the TLs data.

### Effect of pH on TLLs

Fig. 3 illustrates the effect of pH on the TLLs and STLs at the center points of initial concentration of [C<sub>4</sub>mim]BF<sub>4</sub> and organic salts.

It is obvious that the ternary system of [C<sub>4</sub>mim]BF<sub>4</sub> + Na<sub>3</sub>Citrate + water and [C<sub>4</sub>mim]BF<sub>4</sub> + Na<sub>2</sub>Tartrate + water possess the same behaviour. In these systems, the absolute values of STLs increase in the following order (in coded values): pH=0 < pH=-1 < pH=+1. Consequently, by changing the pH in this manner the water is driven from IL-rich phase to the salt-rich phase. However, in ternary system of [C<sub>4</sub>mim]BF<sub>4</sub> + Na<sub>2</sub>Fumarate + water absolute values of STLs increase due to the change of pH according to the following trend: pH=0 < pH=+1 < pH=-1. In this article, we choose [C<sub>4</sub>mim]BF<sub>4</sub>- Na<sub>2</sub>Fumarate ATPS as the basis to represent the graphs as illustrated in Fig. 4.

### 3.4. Effect of Process variables

#### 3.4.1. Effect of feed's initial concentration

In this work, we studied different initial concentrations of [C<sub>4</sub>mim]BF<sub>4</sub> and organic salts to estimate their subsequent effect on biomolecule's partitioning. The complete design matrix along with response values are presented in Table 4. As visualized in response contour plots in Fig. 5a, 5b and 5c, there is a noticeable increase in Cefalexin's partition coefficient with increase in initial concentration of [C<sub>4</sub>mim]BF<sub>4</sub>. This is noticed because the aggregates begin to be more occurring as the IL's initial concentration is increased. Subsequently, the Cefalexin's enrichment is facilitated. Moreover, the same concentration effect is observed for Na<sub>3</sub>Citrate and Na<sub>2</sub>Tartrate organic salts. This effect is reasonable. As the salt concentration is increased the space of the bottom phase is more packed thus, Cefalexin is driven to the top phase.

On the other hand, K<sub>cef</sub> increases as Na<sub>2</sub>Fumarate's initial concentration is changed from 5 wt% to 5.5 wt% but, it decreases again as concentration varies from 5.5 wt% to 6 wt%. The water content of the aqueous solution of Cefalexin affects its structure as a hydration layer is formed on its surface. With increase in the initial concentration of Na<sub>2</sub>Fumarate the bottom phase is more hydrophilic. Consequently, water is driven from the top phase to the bottom phase and K<sub>cef</sub> is reduced. A recent study by Lin et al. reported the same effect by inorganic salt in IL-based ATPS for protein extraction [53]. Therefore, these phenomena indicate the optimum values for feed's initial concentrations.

Salting-in inducing ions usually increase partition coefficient of biomolecule. High charge density ions (salting-out inducing ions) have lower interaction with biomolecule as they tend to form hydration complexes. Contrarily, the salting-in inducing ions have a lower tendency toward formation of hydration complexes, and with formation of specific ions binding to the solute the partition coefficient is increased [54]. The salting-out ability of Citrate<sup>-3</sup> is stronger than Tartrate<sup>-2</sup> and Fumarate<sup>-2</sup>. Thus, it is reasonable to observe the system with Na<sub>3</sub>Citrate having the lowest amount of Cefalexin in its bottom phase compared to others.

#### 3.4.2. Effect of pH

It is a well known fact that the biomolecule's net charge is

dependent on its isoelectric point (pI). Cefalexin is known as an amphoteric compound possessing amino groups and carboxyl group. Its isoelectric point is generally estimated to be 4.5 to 5. Consequently, as the pH of the ATPS is altered the Cefalexin's partitioning between the two phases is affected. In this work, for all the pH that we considered, Cefalexin is favourably partitioned to IL-rich phase.

In IL-Na<sub>3</sub>Citrate and IL-Na<sub>2</sub>Tartrate ATPS, maximum partitioning coefficient is observed at pH=4.5 (Fig. 6a) and pH=4.8 (Fig. 6b), respectively. Since the pI of Cefalexin is between 4.5 to 5, it is predominately a zwitterion (with no net charge) at these pH ranges. At higher pH, which is higher than isoelectric point of Cefalexin, Cefalexin is negatively charged and therefore it tends to remain in organic salt-rich phase. Previous study by Li et al. [55], validates this result. This could be interpreted by the following reasons: Hydrophobic interaction predominantly affects the extraction process and the electrostatic interaction can slightly influence the extraction efficiency [53]. At isoelectric point, strongest hydrophobic interaction and weakest electrostatic interaction is manifested and the optimum Cefalexin's enrichment is observed. The two phases formed in ATPS are of distinct nature. The IL-rich aqueous phase is predominantly a hydrophobic phase, while organic salt-rich phase is more hydrophilic in nature due to the presence of species with high charge density. As a result, the partition coefficient is controlled by the difference in the phases' polarities along with the net-charge of the Cefalexin. A zwitterion preferentially migrates to the most hydrophobic aqueous phase ([C<sub>4</sub>mim]BF<sub>4</sub>-rich phase) while, charged Cefalexin tends to partition for the organic rich hydrophilic phase. The hydrophobic nature of [C<sub>4</sub>mim]BF<sub>4</sub> can be validated by its anions capability to accept proton in hydrogen bond between solute and solvent. The hydrogen-bond basicity (which is determined by solvatochromic probes) for [C<sub>4</sub>mim]BF<sub>4</sub> is 0.38 [56] which justifies its higher hydrophobicity [57]. However, maximum K<sub>cef</sub> for IL-Na<sub>2</sub>Fumarate ATPS is observed at pH=5.5 (see Fig. 6c).

#### 3.4.3. Development of Regression Model equation

A second order polynomial regression equation was developed for evaluation of partition coefficient. These equations represent the effect of independent process variables on the response. Furthermore, we selected the confidence level of 95% for the analysis of RSM and thus, the effects with less than 95% significance were not taken into account. Consequently, the following regression models were evaluated, which are tabulated in the coded values:

#### IL+ Na<sub>3</sub>Citrate ATPS

$$K_{cef} = 1.70 - 0.19x_1 + 0.18x_2 + 0.47x_3 - 0.055x_1x_2 - 0.049x_1x_3 - 0.075x_2x_3 - 0.18x_1^2 + 0.16x_2^2 + 0.28x_3^2 \quad (16)$$

$$R^2 = 0.9671$$

$$\%EE_{cef} = 88.85 - 1.68x_1 - 2.02x_2 + 0.59x_3 - 0.34x_1x_2 - 0.40x_1x_3 + 0.31x_2x_3 - 3.37x_1^2 + 1.32x_2^2 + 1.80x_3^2 \quad (17)$$

$$R^2 = 0.9652$$

**IL+ Na<sub>2</sub>Tartrate ATPS**

$$K_{\text{cef}} = 2.68 - 0.17x_1 + 0.69x_2 + 0.22x_3 - 0.2x_1x_2 - 0.25x_1x_3 - 0.089x_2x_3 + 0.14x_1^2 + 0.3x_2^2 - 0.26x_3^2 \quad (18)$$

$$R^2 = 0.9791$$

$$\%EE_{\text{cef}} = 95.99 - 0.41x_1 + 0.099x_2 - 0.2x_3 - 0.29x_1x_2 - 0.37x_1x_3 - 0.014x_2x_3 - 1.02x_1^2 + 0.36x_2^2 - 0.21x_3^2 \quad (19)$$

$$R^2 = 0.9116$$

**IL+ Na<sub>2</sub>Fumarate ATPS**

$$K_{\text{cef}} = 4.25 - 0.16x_1 + 0.30x_2 + 0.35x_3 - 0.048x_1x_2 - 0.068x_1x_3 - 0.051x_2x_3 - 1.20x_1^2 - 0.42x_2^2 + 0.55x_3^2 \quad (20)$$

$$R^2 = 0.9248$$

$$\%EE_{\text{cef}} = 96.69 - 5.02E^{-3}x_1 - 1.11x_2 - 0.49x_3 - 0.049x_1x_2 - 0.15x_1x_3 + 0.2x_2x_3 - 1.94x_1^2 - 0.17x_2^2 + 0.57x_3^2 \quad (21)$$

$$R^2 = 0.9502$$

In these regression models, positive sign in front of the term shows that the effect of a factor is positive and consequently the  $K_{\text{cef}}$  increases as the factor is changed from low to high levels. On the other hand, if the effect is negative, a reduction in  $K_{\text{cef}}$  is observed for high level of the same factor.

Each regression equation has a  $R^2$ -value, the closer the  $R^2$ -value to unity, the more promising the model will be. The  $R^2$ -value for equations 16, 18 and 20 was 0.9671, 0.9791 and 0.9248, respectively. This indicated that *e.g.* 96.71% of total variation in Cefalexin's partitioning in IL- Na<sub>3</sub>Citrate ATPS could be attributed to the experimental variables studied. All regression equations showed relatively high  $R^2$  value, which was a mere indication of a good agreement between the experimental and predicted  $K_{\text{cef}}$ .

We employed the analysis of variance (ANOVA) for evaluation of the statistical significance of the regression model. The F-test and p-values for all the linear, quadratic and interaction effects are given in Tables 10, 11 and 12 for each IL-organic salt ATPS. Based on the ANOVA analysis for all the systems, the models F-values imply the significance of the models.

In extraction of Cefalexin using IL- Na<sub>3</sub>Citrate ATPS, the linear effects of all independent factors were highly significant (p-value < 0.05). On the other hand, for this system, the interaction effects did not appear to be significant and the only significant quadratic effect was for IL's initial concentration. When employing IL- Na<sub>2</sub>Tartrate, a second order polynomial equation could model  $K_{\text{cef}}$  with significant linear, interaction and quadratic terms (the only insignificant terms were IL × salt and pH<sup>2</sup>). However, only initial concentration of IL and salt along with

quadratic effect of pH and IL's wt% had significant effect on  $K_{\text{cef}}$  in Na<sub>2</sub>Fumarate based ATPS.

**3.5. Optimization Procedure**

In optimization procedure we look for a combination of factor levels that satisfy the requirements placed on responses and factors. Hence, the desired goal for each independent variable (pH, feed's initial concentrations) and response (partition coefficient of Cefalexin) should be selected. The possible choices for goals are either maximize, minimize, target, within range or an exact value. Consequently, an overall desirability function is generated by combination of the goals. Finally, the goal seeking is initiated and two or more maximums can be found due to the curvature nature of the response surfaces and their combination into desirability function.

For optimization purposes, the desired goal for the partition coefficient and the extraction efficiency was chosen to be within a maximum, along with three independent variables to be within range. The optimization results are presented in Table 13.

**3.6. Conductivity and DLS**

It is crucial to investigate the microstructure of the top phase to validate the presence of the aggregates in the IL-rich top phase. The conductivity measurements of various concentrations of IL solution were conducted at 25 ± 1 °C. With the initial increase of concentration rapid increase in the conductivity was observed, and later the curve tended toward stability. The concentration at which two linear fragments intersect is appointed as the critical aggregation concentration (CAC). Close examination of Fig. 7 gives the CAC value of [C<sub>4</sub>mim]BF<sub>4</sub> as 0.156 gr/mL. Knowing the fact that CAC was lower than the top phase concentrations of all the studied ATPS, it is reasonable to conclude that IL aggregates were formed in the top phase. Bowers et al. [58] have conducted conductivity measurements to evaluate the CAC to be 820 ± 100 mmol/dm<sup>3</sup>, which is in agreement to our experimental results.

Fig. 8, illustrates the DLS results of Cefalexin solution along with Cefalexin in IL rich top phase. A wider aggregation peak appeared in range of 20-500 nm, which is noticeably wider than original peak of antibiotic (Fig. 8c). This can be due to the fact that the hydrophobic interactions between the [C<sub>4</sub>mim]BF<sub>4</sub> and Cefalexin can lead to the formations of aggregates which is the main driving force for Cefalexin enrichment in IL-rich phase.

Furthermore, in analysis of the top phase, another intensity aggregation was noticed in the range 1000-10000 nm. This can be interpreted by the formation of aggregates by excess of ionic liquid.

In order to elucidate the microstructure of Cefalexin in IL rich top phase, it is essential to study the aggregation behavior of [C<sub>4</sub>mim]BF<sub>4</sub> aqueous solution. Many studies have focused on the aggregation behavior of the aqueous solutions of ILs [58, 59]. Bowers et al. [58] proposed that the aqueous solution of short chain [C<sub>4</sub>mim]BF<sub>4</sub> can be modeled as a dispersion of polydisperse spherical aggregates. They have also stated that [C<sub>4</sub>mim]BF<sub>4</sub> behaves like short-chain cationic surfactant. Singh et al. [59] observed by NMR- measurements that the imidazole ring of [C<sub>4</sub>mim]BF<sub>4</sub> is positioned at the aggregate surface in a configuration favorable for ring stacking through π-π interaction. Consequently, hydrophobic interactions and π-π conjugation

between imidazole ring of IL and amino group of Cefalexin lead to formation of aggregates.

### 3.7. FT-IR spectroscopy

FT-IR spectra are a useful tool for identification of functional groups or chemical bonds in a molecule or an interaction system [31, 35]. Fig. 9, shows the FT-IR spectra of pure  $[C_4mim]BF_4$ , pure Cefalexin and Cefalexin in  $[C_4mim]BF_4$ . The major peaks in pure Cefalexin are at 1759.16 (C=O stretching), 1596.17 (C=C bending), 1689.71 (C=O stretching), 3420.91 (N-H stretching), 3055.85 (O-H stretching), 2615  $cm^{-1}$  (S-H stretching), 1195.01 (C-N stretching) and 1280.48  $cm^{-1}$  (C-O stretching).

Moreover, the two major absorption bands of Cefalexin (1759.16 and 1596.17  $cm^{-1}$ ) have remained unchanged after its enrichment in IL-organic salt ATPS (Fig. 9c). Thus, it can be concluded that the structural features of Cefalexin before and after extraction are identical. Thereof, by comparison of Fig. 9b and 9c, it is confirmed that no chemical bonds have been formed between Cefalexin and  $[C_4mim]BF_4$ .

### 3.8. TEM

Comprehension of the separation process requires close examination of the IL-rich top phase. Consequently, TEM images of Cefalexin in the IL-rich top phase, the top phase of ATPS without the addition of Cefalexin and aqueous solution of Cefalexin have been examined. The IL-rich top phase is not microscopically homogenous but, it forms a polydisperse solution. Fig. 10a, demonstrates the conformation of non extractive IL-rich top phase and the spot may be attributed to the  $[C_4mim]BF_4$  without too much aggregation. Moreover, Fig. 10b shows pure Cefalexin aqueous solution and Fig. 10c and d, are its TEM images after extraction in top phase of IL-based ATPS. New aggregates are formed after the extraction of antibiotic in  $[C_4mim]BF_4$ -rich top phase. Thereof, there is consistency in size of the aggregates in TEM and DLS. Therefore, it can be stated that the formation of IL aggregates and IL-Cefalexin aggregates is the main driving force in its uptake by IL-organic salt ATPS.

## 4. Conclusion

Biomolecules extraction and purification with application of IL-inorganic salts ATPS have been widely exploited; yet the environmental impacts of these high charge density salts make their use unfavourable. For development of more biocompatible systems, organic salts were chosen as the main constituent of IL-based ATPS. Binodal curves of a common ionic liquid and different organic salts have been studied. The experimental binodal data were satisfactorily correlated by a four parameter equation. It was found that two-phase area would be expanded with increase in the charge of the anions. In addition, effects of systems' parameters on partition coefficients and extraction efficiencies of Cefalexin were estimated by the use of RSM based on three-variable CCD. We also estimated TLs for each experimental run and confirmed their validity by models. Consequently, the regression models and analysis of variance evaluated the factors' subsequent effects on  $K_{cef}$ . Hydrophobic interaction along with salting-out effect and electrostatic interaction governs the transfer process. FT-IR, DLS, conductivity and TEM were used to attain the mechanism of

extraction and microscopic structure of the solution. FT-IR spectra validated that no chemical bonds have been formed between Cefalexin and  $[C_4mim]BF_4$ . Withal, DLS, conductivity and TEM results confirmed the formation of some clusters. To sum up, these results gave us some insight into understanding the behavior of antibiotic in IL-organic salt ATPS.

## Notes and references

<sup>a</sup> Chemical Engineering Department, Amirkabir University of Technology (Tehran Polytechnic), Tehran, Iran.

\* Corresponding author; E-mail: [banana@aut.ac.ir](mailto:banana@aut.ac.ir)

† Electronic Supplementary Information (ESI) available: [details of any supplementary information available should be included here]. See DOI: 10.1039/b000000x/

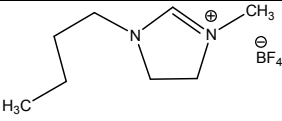
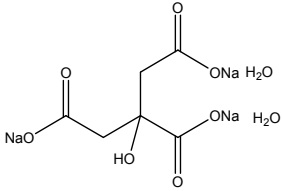
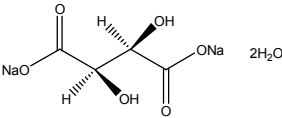
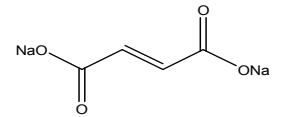
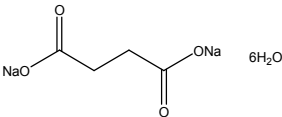
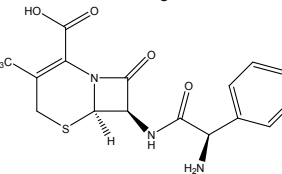
- H. Passos, A. R. Ferreira, A. Filipa, M. Cláudio, *Biochemical Engineering Journal*, 2012, **67**, 68–76.
- S. Abdollahimi, B. Nasernejad and G. Pazuki, *Journal of Molecular Liquids*, 2014, **191**, 79-84.
- M. G. Freire, A. Filipa and M. Claudio, *Chemical Society Reviews*, 2012, **41**, 4966-4995.
- R. Hatti-Kaul, *Aqueous two-phase systems: methods and protocols*, Humana press, Totowa, New Jersey, 2000.
- P.A. Albertsson, *Partitioning of Cell Particles and Macromolecules*, 3rd ed., Wiley, New York, 1986.
- P.P. Madeira, X. Xu, J.A. Teixeira and E.A. Macedo, *Biochemical Engineering Journal*, 2005, **24**, 147–155.
- N. L. P. Dallora, J.G.D. Klemz, P. A. Pessôa Filho, P. P. Madeira, X. Xu, J. A. Teixeira, E. A. Macedo, *Biochemical Engineering Journal*, 2007, **34**, 92–97.
- B.K. Vaidya, H.K. Suthar, S. Kasture, S. Nene, *Biochemical Engineering Journal*, 2006, **28**, 161–166.
- H. Yue, Q. Yuan, W. Wang, *Biochemical Engineering Journal*, 2007, **37**, 231–237.
- G.A. Gomes, A.M. Azevedo, M.R. Aires-Barros and D.M.F. Prazeres, *Separation and Purification Technology*, 2009, **65**, 22–30.
- A. M. Azevedo, A. G. Gomes, P. A. J. Rosa, I. F. Ferreira, A.M.M.O. Pisco and M. R. Aires- Barros, *Separation and Purification Technology*, 2009, **65**,14–21.
- K. E. Gutowski, G. A. Broker, H. D. Willauer, J. G. Huddleston, R. P. Swatloski, J. D. Holbrey and R. D. Rogers, *Journal of the American Chemical Society*, 2003, **125**, 6632–6633.
- S. P. M. Ventura, S. G. Sousa, L. S. Serafim, A. S. Lima, M. G. Freire and J. A. P. Coutinho, *Journal of Chemical Engineering Data*, 2012, **57**, 507–512.
- S. P. M. Ventura, S. G. Sousa, L. S. Serafim, A. S. Lima, M. G. Freire and J. A. P. Coutinho, *Journal of Chemical Engineering Data*, 2011, **56**, 4253–4260.
- S. Dreyer and U. Kragl, *Biotechnology and Bioengineering*, 2008, **99**, 1416-1424.



16. M. G. Freire, C. L. S. Louros, L. P. N. Rebelo and J. A. P. Coutinho, *Green Chemistry*, 2011, **13**, 1536–1545.
17. J. Han, Y. Wang, Y. F. Li, C. L. Yu and Y. S. Yan, *Journal of Chemical Engineering Data*, 2011, **56**, 3679–3687.
18. M. Dominguez-Perez, L. I. N. Tome, M. G. Freire, I. M. Marrucho, O. Cabeza and J. A. P. Coutinho, *Separation and Purification Technology*, 2010, **72**, 85–91.
19. N. J. Bridges, K. E. Gutowski and R. D. Rogers, *Green Chemistry*, 2007, **9**, 177–183.
20. Y. C. Pei, J. J. Wang, L. Liu, K. Wu and Y. Zhao, *Journal of Chemical Engineering Data*, 2007, **52**, 2026–2031.
21. C. M. S. S. Neves, S. P. M. Ventura, M. G. Freire, I. M. Marrucho and J. A. P. Coutinho, *Journal of Physical Chemistry B*, 2009, **113**, 5194–5199.
22. S. P. M. Ventura, C. M. S. S. Neves, M. G. Freire, I. M. Marrucho, J. Oliveira and J. A. P. Coutinho, *Journal of Physical Chemistry B*, 2009, **113**, 9304–9310.
23. J. Han, C. Yu, Y. Wang, X. Xie, Y. Yan, G. Yin and W. Guan, *Fluid Phase Equilibria*, 2010, **295**, 98–103.
24. M. T. Zafarani-Moattar and S. Hamzehzadeh, *Journal of Chemical Engineering Data*, 2009, **54**, 833–841.
25. J. A. Han, R. Pan, X. Q. Xie, Y. Wang, Y. S. Yan, G. W. Yin and W. X. Guan, *Journal of Chemical Engineering Data*, 2010, **55**, 3749–3754.
26. R. Sadeghi, R. Golabiazar and H. Shekaari, *Journal of Chemical Thermodynamics*, 2010, **42**, 441–453.
27. M. T. Zafarani-Moattar and S. Hamzehzadeh, *Journal of Chemical Engineering Data*, 2010, **55**, 1598–1610.
28. M. T. Zafarani-Moattar and S. Hamzehzadeh, *Fluid Phase Equilibria*, 2011, **304**, 110–120.
29. K. Ravikumar, S. Ramalingam, S. Krishnan and K. Balu, *Dyes and Pigments*, 2006, **70**, 18–26.
30. G. Box and N. Draper, *Empirical Model Building and Response Surfaces*, John Wiley and Sons, 1987.
31. Q. Zeng, Y. Wang, N. Li, X. Huang, X. Ding, X. Lin, S. Huang and X. Liu, *Talanta*, 2013, **16**, 409–416.
32. P. Li, Z. Du, X. Ma, G. Wang and G. Li, *Journal of Molecular Liquids*, 2014, **192**, 38–43.
33. X. Wang, X. Wei, J. Liu, J. Liu, D. Sun, P. Du and A. Ping, *Fluid Phase Equilibria*, 2013, **347**, 1–7.
34. X. Ding, Y. Wang, Q. Zeng, J. Chen, Y. Huang and K. Xu, *Analytica Chimica Acta*, 2014, **815**, 22–32.
35. J. Chen, Y. Wang, Q. Zeng, X. Ding and Y. Huang, *Analytical Methods*, 2014, **6**, 4067–4076.
36. Xi. Lin, Y. Wang, Q. Zeng, X. Ding and J. Chen, *Analyst*, 2013, **138**, 6445–6453.
37. J. C. Merchuk, B. A. Andrews and J. A. Asenjo, *Journal of chromatography. B, Biomedical sciences and applications*, 1998, **711**, 285–293.
38. M. Elibol, *Process Biochemistry*, 2002, **67**, 667–773.
39. R.H. Myers, D.C. Montgomery, *Response surface methodology: Process and product optimization using designed experiments*, second ed., John Wiley and Sons, 2002.
40. D. C. Montgomery, *Design and analysis of experiments*, fourth ed., John Wiley and Sons, 1996.
41. K. D. Collins, M. W. Q. Washbaugh, *Quarterly Reviews of Biophysics*, 1985, **18**, 323–422.
42. M. G. Cacace, E. M. Landau and J. J. Ramsden, *Quarterly Reviews of Biophysics*, 1997, **30**, 241–278.
43. M. Holz, R. Grunder, A. Sacco and A. Meleleo, *Journal of the Chemical Society, Faraday Transactions*, 1993, **89**, 1215–1222.
44. M. G. Freire, P. J. Carvalho, A. M. S. Silva, L. M. N. B. F. Santos, J. A. P. Coutinho, *Journal of Physical Chemistry B*, 2009, **113**, 202–211.
45. M. G. Freire, C. M. S. S. Neves, A. M. S. Silva, L. M. N. B. F. Santos, I. M. Marrucho, L. P. N. Rebelo, J. K. Shah, E. J. Maginn and J. A. P. Coutinho, *Journal of Physical Chemistry B*, 2010, **114**, 2004–2014.
46. L. I. N. Tome, F. R. Varanda, M. G. Freire, I. M. Marrucho and J. A. P. Coutinho, *Journal of Physical Chemistry B*, 2009, **113**, 2815–2825.
47. Y. Guan, T. Lilley, T. H. Treffry, *Macromolecules*, 1993, **26**, 3971–3979.
48. J. Han, Y. Wang, C. Yu, Y. Li, W. Kang and Y. Yan, *Journal of Chemical Thermodynamics*, 2012, **45**, 59–67.
49. X. Xie, J. Han, Y. Yan, G. Yin and W. Guan, *Journal of Chemical and Engineering Data*, 2010, **55**, 4741–4745.
50. J. G. Huddleston, H. D. Willauer and R. D. Rogers, *Journal of Chemical and Engineering Data*, 2003, **48**, 1230–1236.
51. D.F. Othmer and P.E. Tobias, *Journal of Industrial and Engineering Chemistry*, 1942, **34**, 690–692.
52. G. Tubio, L. Pellegrini, B. B. Nerli and G. A. Pico, *Journal of Chemical Engineering Data*, 2006, **51**, 209–212.
53. Xi. Lin, Y. Wang, Q. Zeng, X. Ding and J. Chen, *Analyst*, 2013, **138**, 6445–6453.
54. A. Filipa M. Claudio, M. G. Freire, C. S.R. Freire, A.J.D. Silvestre, J. A.P. Coutinho, *Separation and Purification Technology*, 2010, **75**, 39–47.
55. Y. F. Li, J. Han, Y. Wang, J. J. Ma and Y. S. Yan, *Journal of Chemistry*, 2013, **2013**, 1–5.
56. A. Filipa M. Claudio, A. M. Ferreira, S. Shahriari, M. G. Freire and J. A. P. Coutinho, *Journal of Physical Chemistry B*, 2011, **115**, 11145–11153.
57. A. Filipa M. Claudio, A. M. Ferreira, C.S.R. Freire, A. J.D. Silvestre, M. G. Freire and J. A.P. Coutinho, *Separation and Purification Technology*, 2012, **97**, 142–149.

- 
58. J. Bowers, C. P. Butts, P. J. Martin, and M. C. Vergara-Gutierrez, *Langmuir*, 2004, **20**, 2191-2198.
59. T. Singh, A. Kumar, *Journal of Physical Chemistry B*, 2007, **111**, 7843-7851.
- 30
- 35
- 40
- 45
- 50
- 55

**Table 1** Detailed properties of studied materials

Material	Chemical Formula	Molar Mass (gr mol <sup>-1</sup> )	Source	Chemical Structure	Abbreviations
1-Butyl-3-methylimidazolium tetrafluoroborate	C <sub>8</sub> H <sub>13</sub> BF <sub>4</sub> N <sub>2</sub>	226.02	Synthesized		[C <sub>4</sub> mim]BF <sub>4</sub>
Tri-Sodium citrate 5,5-hydrate	C <sub>6</sub> H <sub>5</sub> Na <sub>3</sub> O <sub>7</sub> * 5,5 H <sub>2</sub> O	357.16	Merck Millipore		Na <sub>3</sub> Citarte
Di-Sodium tartrate dihydrate	C <sub>4</sub> H <sub>4</sub> Na <sub>2</sub> O <sub>6</sub> * 2H <sub>2</sub> O	230.08	Merck Millipore		Na <sub>2</sub> Tartrate
Di-Sodium fumarate	C <sub>4</sub> H <sub>2</sub> Na <sub>2</sub> O <sub>4</sub>	160.04	Merck Millipore		Na <sub>2</sub> Fumarate
Di-Sodium succinate hexahydrate	C <sub>4</sub> H <sub>4</sub> Na <sub>2</sub> O <sub>4</sub> * 6H <sub>2</sub> O	270.15	Merck Millipore		Na <sub>2</sub> Succinate
Cefalexin	C <sub>16</sub> H <sub>17</sub> N <sub>3</sub> O <sub>4</sub> S	347.39	Jaber Ebne Hayyan Company		

5

10

15

20

25

5 **Table 2** Experimental range and levels of independent process variables for Cefalexin extraction in IL-based ATPS

Independent Variables	RANGES AND LEVELS								
	Na <sub>3</sub> Citrate			Na <sub>2</sub> Tartrate			Na <sub>2</sub> Fumarate		
	(-1)	(0)	(+1)	(-1)	(0)	(+1)	(-1)	(0)	(+1)
pH ( $X_1$ )	4.5	5.5	6.5	4.8	5.5	6.2	4.5	5.5	6.5
Organic Salt (wt%) ( $X_2$ )	12	13.5	15	6.8	7.4	8	5	5.5	6
[C <sub>4</sub> mim]BF <sub>4</sub> (wt%) ( $X_3$ )	15	17.5	20	22	24	26	27	29.5	32

10

15

20

25

30

35

40

45

50

**Table 3** Values of parameters (A, B, C and D) of Eq. (1) for the IL-based ATPSs at T=298.15 K

<b>Biphasic System</b>	<i>A</i>	<i>B</i>	<i>C</i>	<i>D</i>	<i>R</i> <sup>2</sup>	100 <i>sd</i>
[C <sub>4</sub> mim]BF <sub>4</sub> +Na <sub>3</sub> Citrate	4.6639	-0.6436	0.0038	0.0005	0.9989	0.874
[C <sub>4</sub> mim]BF <sub>4</sub> + Na <sub>2</sub> Tartrate	5.2551	-1.3296	0.1800	-0.0013	0.9998	0.408
[C <sub>4</sub> mim]BF <sub>4</sub> + Na <sub>2</sub> Fumarate	5.3437	-1.3094	0.1613	-0.00095	0.9995	0.754
[C <sub>4</sub> mim]BF <sub>4</sub> + Na <sub>2</sub> Succinate	4.1639	-0.2097	-0.1707	0.0094	0.9998	0.597

$${}^a R^2 = 1 - \frac{\sum_1^N (w_{IL,exp} - w_{IL,pre})^2}{\sum_1^N (w_{IL,exp})^2} \quad ; \quad sd = \left( \frac{\sum_1^N (w_{IL,exp} - w_{IL,pre})^2}{N} \right)^{0.5} ; w_{IL,exp} = \text{Experimental IL wt\%} \quad \text{and} \quad w_{IL,pre} = \text{predicted IL wt\%}$$

10

15

20

25

30

35

40

**Table 4** CCD design matrix along with experimental and predicted response values

Std. Order	$x_1$	$x_2$	$x_3$	Partitioning Coefficient					
				<i>Na<sub>3</sub>Citrate</i>		<i>Na<sub>2</sub>Tartrate</i>		<i>Na<sub>2</sub>Fumarate</i>	
				Experimental	Predicted	Experimental	Predicted	Experimental	Predicted
1	-1	-1	-1	1.2579	1.3210	1.6363	1.5810	2.7073	2.5230
2	1	-1	-1	1.1444	1.1490	2.0948	2.1410	2.6236	2.4350
3	-1	1	-1	2.0082	1.9410	3.4852	3.5390	3.3157	3.3210
4	1	1	-1	1.4943	1.5490	3.2746	3.2990	3.0301	3.0410
5	-1	-1	1	2.5911	2.5090	2.6632	2.6990	3.4714	3.4610
6	1	-1	1	2.1005	2.1410	2.2545	2.2590	3.1052	3.1010
7	-1	1	1	2.8585	2.8290	4.3	4.3010	3.8688	4.0550
8	1	1	1	2.3316	2.2410	2.9375	3.0610	3.3181	3.5030
9	-1	0	0	1.5850	1.7100	3.0061	2.9900	3.2191	3.2100
10	1	0	0	1.3774	1.3300	2.7882	2.6500	2.8817	2.8900
11	0	-1	0	1.7224	1.6800	2.2696	2.2900	3.1722	3.5300
12	0	1	0	1.9187	2.0400	3.8412	3.6700	4.5	4.1300
13	0	0	-1	1.6015	1.5100	2.2031	2.2000	4.0882	4.4500
14	0	0	1	2.2878	2.4500	2.7857	2.6400	5.5232	5.1500
15	0	0	0	1.7922	1.7000	2.5229	2.6800	4.2131	4.2500
16	0	0	0	1.7835	1.7000	2.5114	2.6800	4.275	4.2500

5

10

15

20

25

**Table 5** Values of parameters of EEV of salts using equations (12) or (13) for the [C<sub>4</sub>mim]BF<sub>4</sub> (1) + salt (2) + water (3) ATPS at T=298.15 K

Salt	$V_{213}^*$	$f_{213}$	$R^2$	$100sd$
Na <sub>3</sub> Citrate	14.054		0.997	0.248
Na <sub>2</sub> Succinate	13.800	0.012	0.993	0.130
Na <sub>2</sub> Tartrate	12.459		0.997	0.223
Na <sub>2</sub> Fumarate	10.445		0.998	0.131
Na <sub>3</sub> Phosphate	12.912		0.954	0.352

$$a R^2 = 1 - \frac{\sum_1^N (w_{ll,exp} - w_{ll,pre})^2}{\sum_1^N (w_{ll,exp})^2}; sd = \left( \sum_1^N (w_{ll,exp} - w_{ll,pre})^2 / N \right)^{0.5}, w_{ll,exp} = \text{Experimental IL wt\%} \text{ and } w_{ll,pre} = \text{predicted IL wt\%}$$

5

10

15

20

25

30

35

40

45

**Table 6** Weight fraction percentage (wt%) obtained by DOE for the coexisting phases of  $[\text{C}_4\text{mim}]\text{BF}_4(1)+ \text{Na}_3\text{Citrate} (2)+ \text{H}_2\text{O}$  along with their respective values of STL and TLL<sup>a</sup>

pH	Std. order	Feed		Top phase		Bottom phase		$\alpha$	STL	TLL
		$w_1$	$w_2$	$w_1$	$w_2$	$w_1$	$w_2$			
4.5	1	15	12	16.0549	9.4245	5.506	35.1795	0.8975	-0.405	27.831
	3	15	15	17.7161	8.3735	5.398	38.4258	0.7795	-0.409	32.478
	5	20	12	23.1375	5.9165	5.3845	40.3388	0.8232	-0.515	38.730
	7	20	15	25.1031	5.2683	5.4196	42.8053	0.7407	-0.524	42.384
	9	17.5	13.5	20.5086	6.9601	5.3846	39.836	0.8010	-0.460	36.187
5.5	11	17.5	12	19.3427	7.5051	5.3942	41.5305	0.8678	-0.409	36.773
	12	17.5	15	21.1086	6.701	5.419	42.7835	0.7864	-0.434	39.346
	13	15	13.5	16.6324	9.0374	5.3847	39.7851	0.8548	-0.365	32.740
	14	20	13.5	23.7319	5.7101	5.4527	43.866	0.7958	-0.479	42.308
	15	17.5	13.5	20.137	7.1275	5.4169	42.6993	0.8208	-0.413	38.497
	16	17.5	13.5	20.1197	7.1354	5.4207	42.8463	0.8217	-0.411	38.617
6.5	2	15	12	16.1602	9.352	5.6126	33.4247	0.8754	-0.438	26.282
	4	15	15	18.1077	8.1515	5.4679	36.0063	0.7541	-0.453	30.588
	6	20	12	23.3109	5.8553	5.389	39.1163	0.8152	-0.538	37.782
	8	20	15	25.3865	5.1825	5.3954	41.6186	0.7305	-0.548	41.56
	10	17.5	13.5	20.7084	6.8723	5.3968	38.5021	0.7904	-0.484	35.140

<sup>a</sup> Standard uncertainties  $u$  are  $u(w) = 0.0001$  and  $u(T) = 1K$  and  $u(pH) = 0.01$ .

5

10

15

20

25

30

35

40



**Table 7** Weight fraction percentage (wt%) obtained by DOE for the coexisting phases of [C<sub>4</sub>mim]BF<sub>4</sub>(1)+ Na<sub>2</sub>Tartrate(2)+ H<sub>2</sub>O along with their respective values of STL and TLL

pH	Std.order	Feed		Top Phase		Bottom Phase		$\alpha$	STL	TLL
		$w_1$	$w_2$	$w_1$	$w_2$	$w_1$	$w_2$			
4.8	1	22	6.8	23.0451	5.0942	9.4431	27.2947	0.9231	-0.612	26.036
	3	22	8	24.0593	4.7687	9.342	27.8621	0.8600	-0.637	27.384
	5	26	6.8	28.3082	3.7158	9.0614	29.4337	0.8800	-0.748	32.122
	7	26	8	29.3371	3.5164	8.7448	31.1835	0.8379	-0.744	34.489
	9	24	7.4	26.2102	4.1825	9.1308	29.0458	0.8705	-0.686	30.164
5.5	11	24	6.8	25.4185	4.3838	8.3084	33.5292	0.9170	-0.587	33.796
	12	24	8	26.2262	4.1786	7.9018	35.6336	0.8785	-0.582	36.403
	13	22	7.4	23.3192	5.0026	8.6608	31.6415	0.9100	-0.550	30.405
	14	26	7.4	28.2476	3.7281	7.5046	37.6164	0.8916	-0.612	39.732
	15	24	7.4	25.8141	4.2813	8.0661	34.7928	0.8977	-0.581	35.297
	16	24	7.4	25.8822	4.2637	8.308	33.5312	0.8928	-0.600	34.139
6.2	2	22	6.8	23.2153	5.037	10.0035	24.2024	0.9080	-0.689	23.277
	4	22	8	24.2421	4.7137	9.6589	26.0885	0.8462	-0.682	25.875
	6	26	6.8	28.5012	3.677	9.2612	28.3153	0.8690	-0.780	31.260
	8	26	8	29.4186	3.5013	8.8589	30.5567	0.8337	-0.759	33.980
	10	24	7.4	26.373	4.143	9.423	27.402	0.8607	-0.728	28.784

<sup>s</sup> Standard uncertainties  $u$  are  $u(w) = 0.0001$  and  $u(T) = 1K$  and  $u(pH) = 0.01$ .

10

15

20

25

30

35

40

**Table 8** Weight fraction percentage (wt%) obtained by DOE for the coexisting phases of [C<sub>4</sub>mim]BF<sub>4</sub>(1)+ Na<sub>2</sub>Fumarate(2)+ H<sub>2</sub>O along with their respective values of STL and TLL

pH	Std.order	Feed		Top Phase		Bottom Phase		$\alpha$	STL	TLL
		$w_1$	$w_2$	$w_1$	$w_2$	$w_1$	$w_2$			
4.5	1	27	5	28.3306	4.0648	11.5784	15.8385	0.9205	-1.422	20.475
	3	27	6	30.4305	3.6657	11.2603	16.7101	0.8210	-1.469	23.187
	5	32	5	35.4845	2.9208	10.9888	17.5371	0.8577	-1.675	28.525
	7	32	6	37.7968	2.6536	10.7743	18.2533	0.7854	-1.732	31.202
5.5	9	29.5	5.5	33.0055	3.2542	11.0593	17.3144	0.8402	-1.560	26.063
	11	29.5	5	31.5048	3.4848	10.4687	19.3842	0.9046	-1.323	26.368
	12	29.5	6	33.3085	3.2104	10.3022	20.0617	0.8344	-1.362	28.517
	13	27	5.5	28.9235	3.9454	10.6438	18.7194	0.8947	-1.237	23.503
	14	32	5.5	35.7616	2.8868	10.1616	20.6713	0.8530	-1.439	31.171
	15	29.5	5.5	32.3704	3.3488	10.3531	19.8495	0.8696	-1.334	27.514
6.5	16	29.5	5.5	32.3699	3.3489	10.3526	19.8518	0.8696	-1.334	27.515
	2	27	5	28.1891	4.0942	11.1334	17.0862	0.9302	-1.312	21.440
	4	27	6	30.0848	3.727	10.8559	17.8733	0.8393	-1.357	23.847
	6	32	5	35.1759	2.9595	10.6431	18.7221	0.8705	-1.556	29.160
	8	32	6	37.4017	2.6967	10.5351	19.1265	0.7989	-1.635	31.492
10	29.5	5.5	32.7427	3.2928	10.777	18.244	0.8523	-1.469	26.571	

<sup>a</sup> Standard uncertainties  $u$  are  $u(w) = 0.0001$  and  $u(T) = 1K$  and  $u(pH) = 0.01$ .

10

15

20

25

30

35

40

5 **Table 9** Parameters of Othmer-Tobias and Bancroft equations along with their correlation coefficients  $R^2$  and standard deviations ( $sd$ )

Biphasic System	pH	Othmer-Tobias			Bancroft			$100sd_1$	$100sd_2$
		$a$	$b$	$R^2$	$c$	$d$	$R^2$		
[C <sub>4</sub> mim]BF <sub>4</sub> + Na <sub>3</sub> Citrate	4.5	0.557	1.862	0.906	-0.355	0.547	0.906	1.325	3.209
	5.5	0.636	2.379	0.916	-0.352	0.444	0.915	0.776	1.938
	6.5	0.504	1.689	0.964	-0.391	0.636	0.964	1.037	1.747
[C <sub>4</sub> mim]BF <sub>4</sub> + Na <sub>2</sub> Tartrate	4.8	-0.600	1.826	0.921	0.246	0.523	0.921	0.919	1.551
	5.5	0.497	0.868	0.909	-0.562	1.077	0.910	1.023	1.190
	6.2	-0.052	1.104	0.931	-0.009	0.876	0.931	1.314	1.467
[C <sub>4</sub> mim]BF <sub>4</sub> + Na <sub>2</sub> Fumarate	4.5	-3.417	2.617	0.959	1.192	0.364	0.959	0.742	1.294
	5.5	-2.683	2.440	0.982	0.984	0.406	0.982	0.310	0.557
	6.5	-3.994	3.14	0.967	1.153	0.308	0.967	0.585	1.160

$$sd = \left[ \sum_1^N ((w_{i,j,pre}^{top} - w_{i,j,exp}^{top})^2 - (w_{i,j,pre}^{bot} - w_{i,j,exp}^{bot})^2) / 2N \right]^{0.5}, \text{ where } N \text{ is the number of TLs and } j = 1 \text{ and } j = 2, sd_1 \text{ and } sd_2 \text{ the mass}$$

fraction standard deviation for IL and salt, respectively.

10

15

20

25

30

35

40

5 **Table 10** ANOVA table for the partitioning coefficient of cefalexin in [C<sub>4</sub>mim]BF<sub>4</sub>+ Na<sub>3</sub>Citrate+ water ATPS

---

Source	Sum of squares	DF	Mean Square	F-value	p-value
<b>Model</b>	3.32	9	0.37	19.59	0.0009
<i>IL</i>	0.34	1	0.34	18.23	0.0053
<i>Salt</i>	0.32	1	0.32	17.12	0.0061
<i>PEG</i>	2.17	1	2.17	115.51	0.0001
<i>IL</i> × <i>salt</i>	0.024	1	0.024	1.27	0.3035
<i>IL</i> × <i>PEG</i>	0.019	1	0.019	1.01	0.3536
<i>Salt</i> × <i>PEG</i>	0.045	1	0.045	2.40	0.1720
<i>IL</i> <sup>2</sup>	0.087	1	0.087	4.61	0.0754
<i>salt</i> <sup>2</sup>	0.066	1	0.066	3.49	0.1108
<i>PEG</i> <sup>2</sup>	0.21	1	0.21	11.14	0.0157
<b>Residual</b>	0.11	6	0.019		
<i>Lack of fit</i>	0.11	5	0.023	602.53	0.0309
<i>Pure error</i>	3.748E-5	1	3.748E-5		
<b>Total</b>	3.43	15			

---

10

15

20

25

30

35

40

5

**Table 11** ANOVA table for the partitioning coefficient of cefalexin in [C<sub>4</sub>mim]BF<sub>4</sub>+ Na<sub>2</sub>Tartrate+ water ATPS

Source	Sum of squares	DF	Mean Square	F-value	p-value
<b>Model</b>	6.91	9	0.77	31.26	0.0002
<i>IL</i>	0.30	1	0.30	12.35	0.0126
<i>Salt</i>	4.79	1	4.79	195.09	0.0001
<i>PEG</i>	0.50	1	0.50	20.57	0.0040
<i>IL</i> × <i>salt</i>	0.33	1	0.33	13.41	0.0106
<i>IL</i> × <i>PEG</i>	0.51	1	0.51	20.76	0.0039
<i>Salt</i> × <i>PEG</i>	0.063	1	0.063	2.56	0.1607
<i>IL</i> <sup>2</sup>	0.051	1	0.051	2.08	0.1992
<i>salt</i> <sup>2</sup>	0.23	1	0.23	9.51	0.0216
<i>PEG</i> <sup>2</sup>	0.18	1	0.18	7.46	0.0341
<b>Residual</b>	0.15	6	0.025		
<i>Lack of fit</i>	0.15	5	0.029	445.70	0.0359
<i>Pure error</i>	6.606E-5	1	6.606E-5		
<b>Total</b>	7.05	15			

10

15

20

25

30

35

40

5

**Table 12** ANOVA table for the partitioning coefficient of Cefalexin in [C<sub>4</sub>mim]BF<sub>4</sub>+ Na<sub>2</sub>Fumarate+ water ATPS

Source	Sum of squares	DF	Mean Square	F-value	p-value
<b>Model</b>	8.31	9	0.92	8.20	0.0093
<i>IL</i>	0.26	1	0.26	2.34	0.1768
<i>Salt</i>	0.87	1	0.87	7.75	0.0319
<i>PEG</i>	1.24	1	1.24	11.02	0.0160
<i>IL</i> × <i>salt</i>	0.019	1	0.019	0.17	0.6980
<i>IL</i> × <i>PEG</i>	0.037	1	0.037	0.33	0.5850
<i>Salt</i> × <i>PEG</i>	0.020	1	0.020	0.18	0.6847
<i>IL</i> <sup>2</sup>	3.82	1	3.82	33.92	0.0011
<i>salt</i> <sup>2</sup>	0.46	1	0.46	4.09	0.0896
<i>PEG</i> <sup>2</sup>	0.80	1	0.80	7.13	0.0370
<b>Residual</b>	0.68	6	0.11		
<i>Lack of fit</i>	0.67	5	0.13	70.35	0.0903
<i>Pure error</i>	1.915E-3	1	1.915E-3		
<b>Total</b>	8.99	15			

10

15

20

**Table 13** Optimum operating conditions of the process variables for maximum partitioning coefficient at T=298.15 K

Biphasic System	Optimum Level				
	<i>pH</i>	<i>IL wt%</i>	<i>Salt wt%</i>	$K_{Cef}$	% $EE_{Cef}$
[C <sub>4</sub> mim]BF <sub>4</sub> +Na <sub>3</sub> Citrate	5.15	20	15	2.7935	91.0152
[C <sub>4</sub> mim]BF <sub>4</sub> + Na <sub>2</sub> Tartrate	4.97	24.83	8	4.1199	96.3911
[C <sub>4</sub> mim]BF <sub>4</sub> + Na <sub>2</sub> Fumarate	5.45	32	5.36	5.0639	97.0062

5

10

15

20

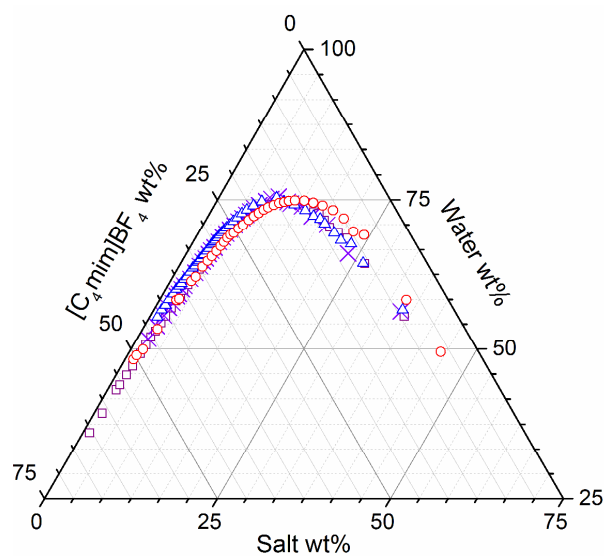


**Fig. 1** Evaluation of the organic salts' effects in the ternary phase diagrams composed of [C<sub>4</sub>mim]BF<sub>4</sub>+sodium based organic salt + H<sub>2</sub>O:  $\triangle$  Na<sub>3</sub>Citrate;  $\circ$ , Na<sub>2</sub>Succinate;  $\times$ , Na<sub>2</sub>Tartrate; and  $\square$ , Na<sub>2</sub>Fumarate

5

10

15

20



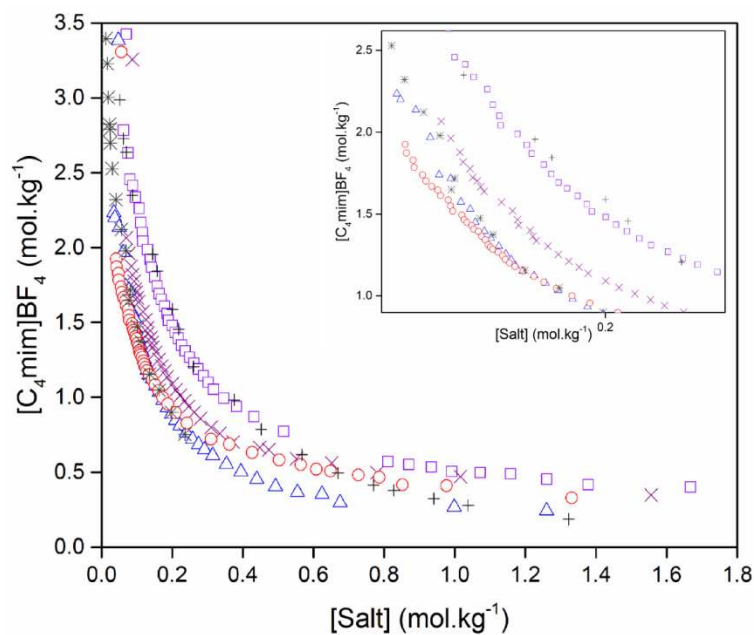


**Fig. 2** Ternary phase diagrams for  $[C_4mim]BF_4$ +sodium based organic salt +  $H_2O$  at 298 K and atmospheric pressure in molality units:  $\triangle$   $Na_3Citrate$ ;  $*$ ,  $Na_3Phosphate$ ;  $\circ$ ,  $Na_2Succinate$ ;  $\times$ ,  $Na_2Tartrate$ ;  $+$ ,  $Na_2Carbonate$  and  $\square$ ,  $Na_2Fumarate$

5

10

15

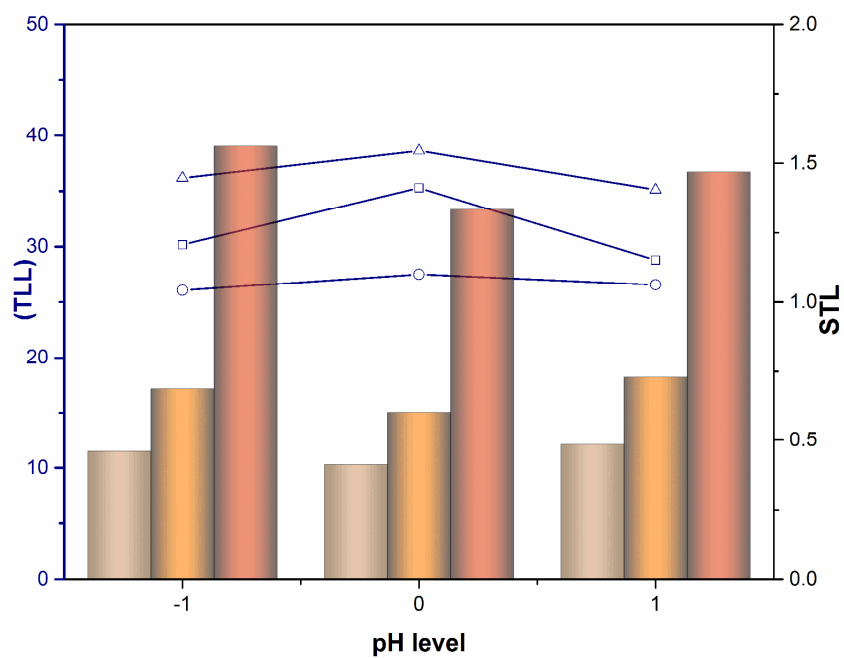


**Fig. 3** Effect of pH on TLLs and STLs in center point of IL and organic salts initial concentration in DOE table. TLL:  $\triangle$ , Na<sub>3</sub>Citrate;  $\square$ , Na<sub>2</sub>Tartrate; and  $\circ$ , Na<sub>2</sub>Fumarate. SLL:  $\square$ , Na<sub>3</sub>Citrate;  $\square$ , Na<sub>2</sub>Tartrate; and  $\square$ , Na<sub>2</sub>Fumarate.

5

10

15

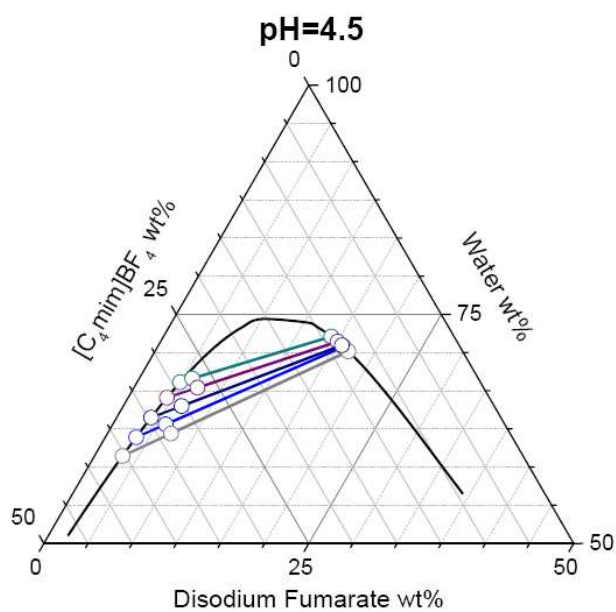
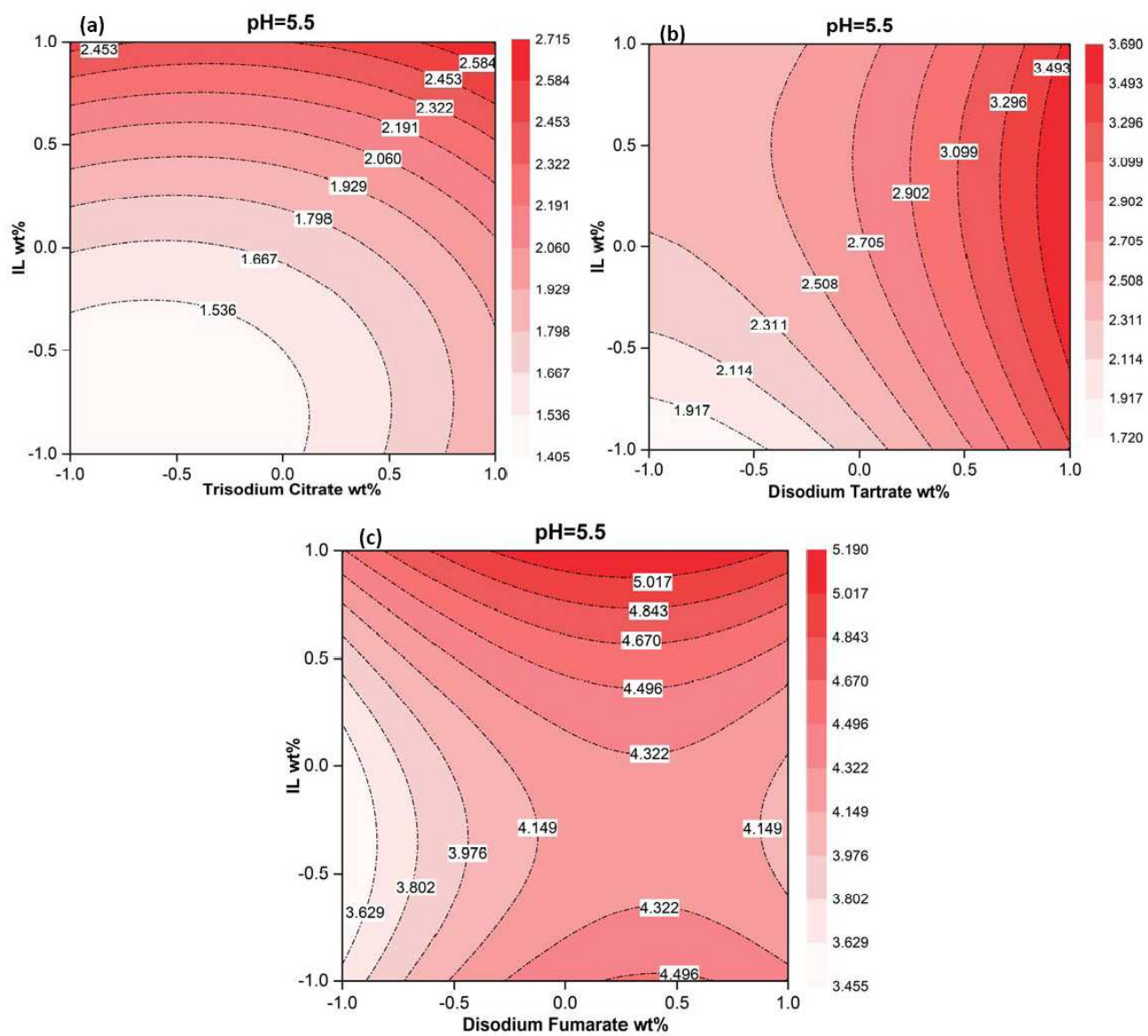


Fig. 4 Demonstration of Tie-lines for  $[\text{C}_4\text{mim}]\text{BF}_4 + \text{Na}_2\text{Fumarate} + \text{H}_2\text{O}$  ATPS at  $\text{pH}=4.5$

5



**Fig. 5** Contour plots of effects of initial concentrations of organic salts and IL on partitioning coefficient of Cefalexin (a)  $\text{Na}_3\text{Citrate}$ , (b)  $\text{Na}_2\text{Tartrate}$  and (c)  $\text{Na}_2\text{Fumarate}$

5

10

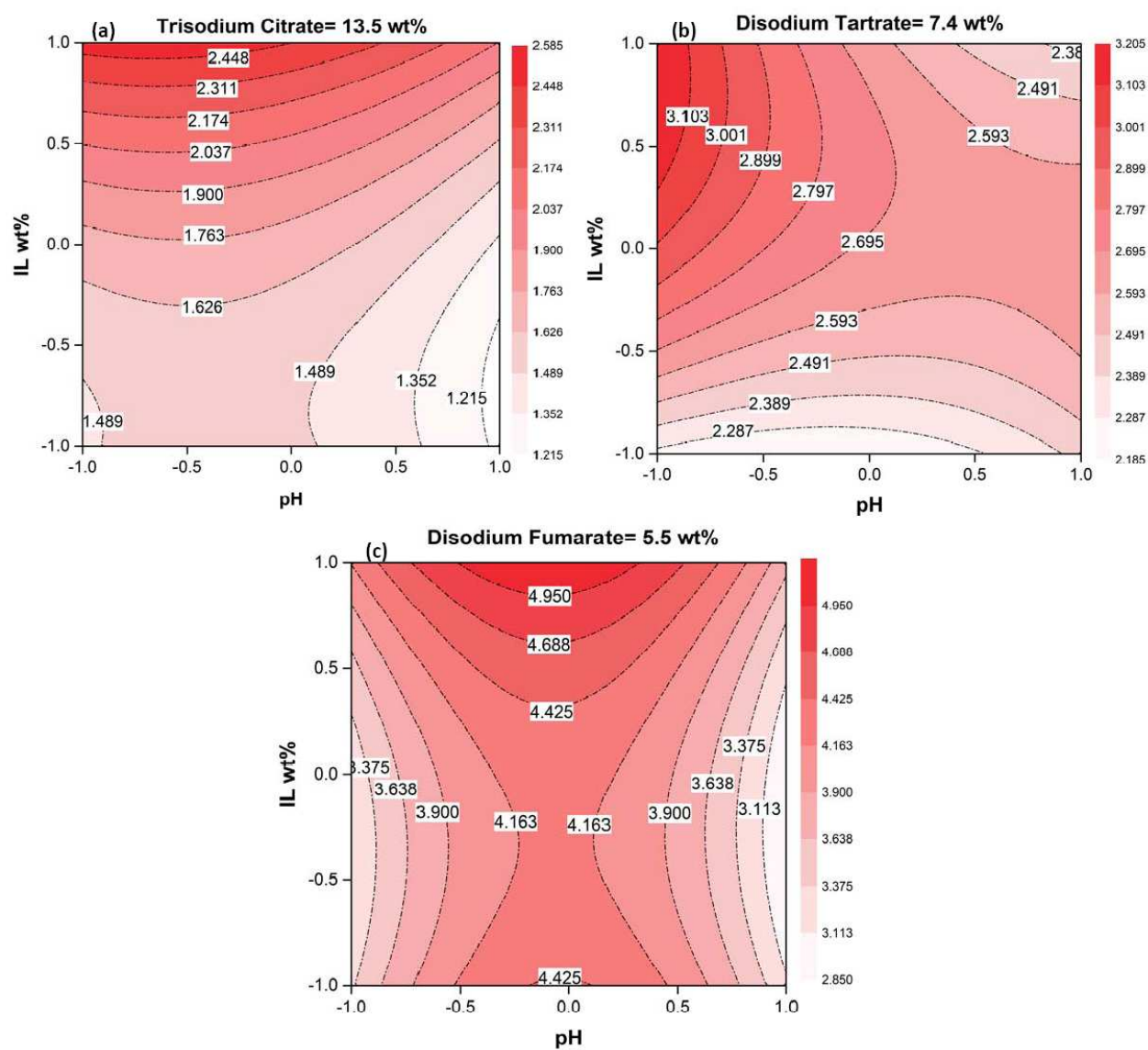


Fig. 6 Contour plots of effects of initial concentrations of IL and pH on partitioning coefficient of Cefalexin (a)  $\text{Na}_3\text{Citrate}$ , (b)  $\text{Na}_2\text{Tartrate}$  and (c)  $\text{Na}_2\text{Fumarate}$

5

10

15

20

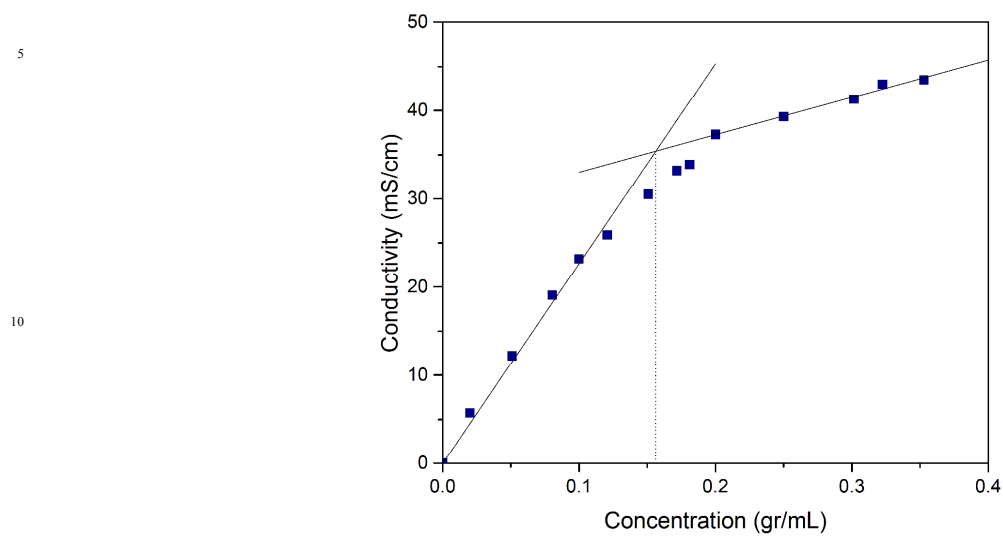


**Fig. 7** The concentration dependence of the conductivity for  $[\text{C}_4\text{mim}]\text{BF}_4$  in aqueous solutions at  $25\pm 1^\circ\text{C}$ .

15

20

25

30

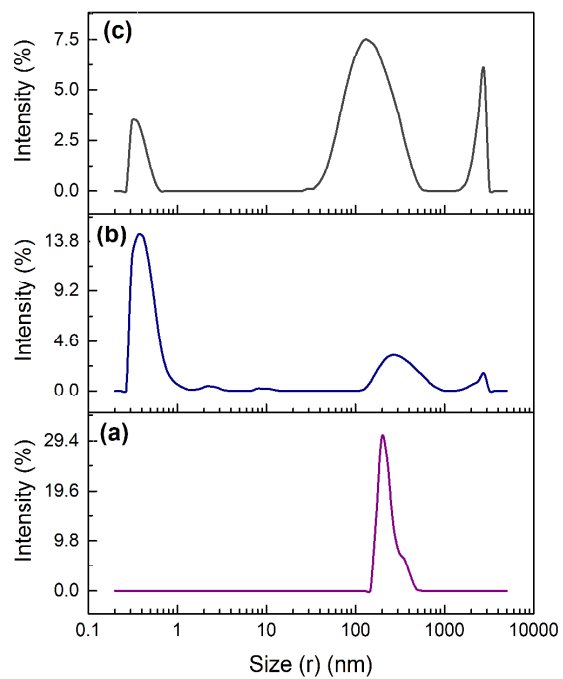


**Fig. 8** DLS graph (a) pure aqueous solution of Cefalexin, (b) IL rich upper phase without Cefalexin and (c) Cefalexin in IL rich top phase

5

10

15

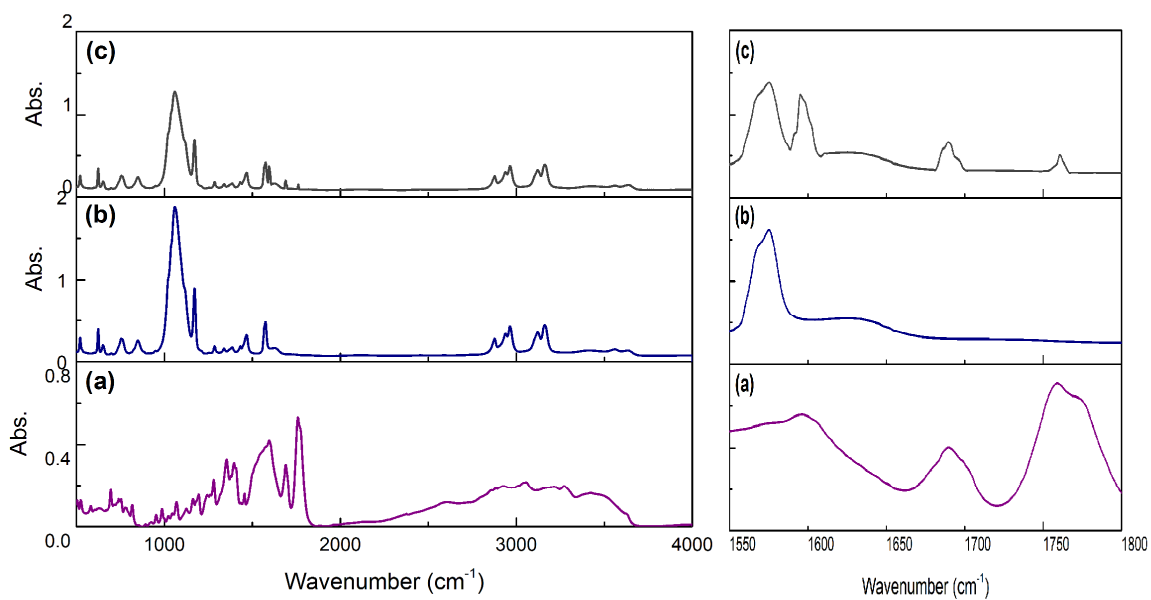


**Fig. 9** FT-IR spectra of pure Cefalexin, pure [C<sub>4</sub>mim]BF<sub>4</sub> and Cefalexin in [C<sub>4</sub>mim]BF<sub>4</sub>. (a) Pure Cefalexin; (b) pure [C<sub>4</sub>mim]BF<sub>4</sub>; (c) Cefalexin in [C<sub>4</sub>mim]BF<sub>4</sub>

5

10

15



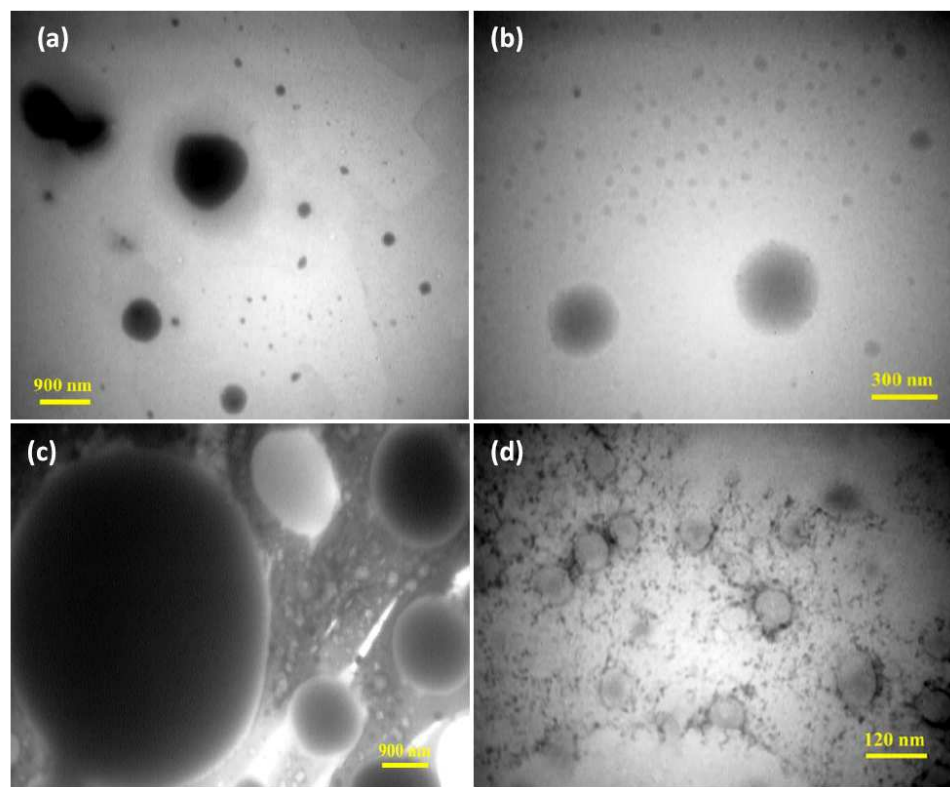


**Fig. 10** TEM images (a) IL rich upper phase without Cefalexin, (b) pure aqueous solution of Cefalexin, (c) and (d) Cefalexin in IL rich top phase

5

10